Wireless Anti-Stokes Photo-induced Electrochemiluminescence at Closed Semiconducting Bipolar Electrodes

Yiran Zhao, Julie Descamps, Brieg Le Corre, Yoan Léger, Alexander Kuhn, Neso Sojic, Gabriel Loget

Wireless Anti-Stokes Photo-induced Electrochemiluminescence at Closed Semiconducting Bipolar Electrodes

Yiran Zhao,[a] *Julie Descamps,*[b] *Brieg le Corre,*[c] *Yoan Léger,*[c] *Alexander Kuhn,*[b] *Neso Sojic,*[b,]* *Gabriel Loget*[a,]*

a. Univ Rennes, CNRS, ISCR (Institut des Sciences Chimiques de Rennes)-UMR6226 Rennes F-35000, France.

*gabriel.loget@cnrs.fr

b. University of Bordeaux, CNRS, Bordeaux INP, ISM, UMR CNRS 5255 Pessac 33607, France.

*neso.sojic@enscbp.fr

c. Univ Rennes, INSA Rennes, CNRS, Institut FOTON-UMR 6082, F-35000, Rennes, France.

ABSTRACT: Wireless electrochemical systems constitute a rapidly developing field. Herein, photo-induced electrochemiluminescence (PECL) is studied at Si-based closed bipolar electrodes (BPEs) for designing anti-Stokes systems that can convert IR into visible photons, without direct electrical contact. We show that protection of the anodic emitting pole of the BPE allows the triggering of bright and longstanding emission under the synergetic actions of an external bias and IR illumination. Photoactive *n*- and *p*-type Si BPEs are studied with front-side and back-side illumination, respectively, and non-photoactive n^+-Si BPEs are studied in the dark. Two electrochemiluminescent (ECL) systems ($[Ru(bpy)_3]^{2+}$/TPrA and L-012) are tested and we show that the onset bias and the anti-Stokes shift can be controlled by the ECL system that is employed. These advances, rationalized by simulations, will be useful for the design of original PECL systems for chemical sensing or photodetection.

TOC GRAPHICS

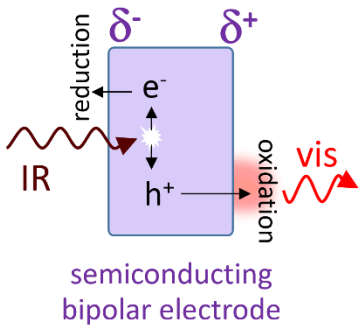

KEYWORDS. Photoelectrochemistry, Electrochemiluminescence, Bipolar Electrochemistry, Semiconductors, Silicon

Photoelectrochemistry at semiconductors (SCs) is a field of research that studies light-absorbing SC photoelectrodes immersed in an electrolyte.[1–3] Upon absorption of incident photons with an energy higher than the SC's bandgap, minority charge carriers reach the SC/electrolyte interface and participate in electrochemical reactions. This field has been widely developed in the frame of solar energy conversion.[4–6] On the other hand, electrochemiluminescence (ECL), also called electrogenerated luminescence, is the emission of photons by electrochemical means, generally involving the electrochemical formation of the excited state of a luminophore at the surface of an electrode.[7,8] It has well-established applications in the biomedical field[9–11] and can be considered as an opposite process of SC photoelectrochemistry because, in this case, the electrode does not absorb light, but acts as an emitter. Interestingly, the photons produced by ECL can be used to trigger photoelectrochemistry at SCs.[12,13] Conversely, ECL can be triggered at the surface of an illuminated SC photoelectrode via a mechanism referred to as photo-induced ECL (PECL).[14] Taking advantage of the absorption properties of the different SC materials and emission properties of ECL luminophores, PECL can be employed to convert light in different ways.[15–21] For instance, it can be used to perform anti-Stokes conversion of IR into visible radiation at low applied potentials by using a narrow bandgap photoelectrode (such as Si) and an ECL system emitting visible light.[19–21]

Bipolar electrochemistry is a fundamentally different wireless electrochemical technique, compared to classic electrochemistry, that induces electron-transfer reactions with spatial control on the surface of a conducting object.[22,23] This technique contrasts with the usual 2- or 3-electrode setups employed in conventional electrochemical experiments because, in bipolar electrochemistry, the electrode of interest is immersed in the electrolyte without any wire

connection. Instead, two external feeder electrodes connected to a power supply are located on either side of the conductive object to generate a potential drop in the electrolyte. At a sufficiently high potential drop, oxidation and reduction take place simultaneously at the poles of the conducting object, referred to as bipolar electrode (BPE).[24] Over the last decade, bipolar electrochemistry has become a unique approach for micro- and nanostructuration,[25–27] motion generation,[28] and electroanalysis.[29,30] Bipolar electrochemistry can be achieved in two main configurations, referred to as open and closed bipolar cells. In open bipolar cells, the BPE is positioned between the feeder electrodes which are immersed in the same electrolyte. In closed bipolar cells, the BPE separates the cell into two compartments, each containing a feeder electrode, allowing for employing different electrolytes.[31] Bipolar electrochemistry has been coupled with photoelectrochemistry at SCs for the design of Boolean logic gates[32–34] and selective electrodeposition.[35,36] It has been coupled to ECL for sensing,[30,37–41] motion tracking,[42,43] and imaging.[44–47] In this letter, Si-based photoactive BPEs are investigated for the generation of upconversion PECL in a closed bipolar cell. We show that anodic anti-Stokes PECL can be triggered wirelessly on bipolar electrodes composed of *n*- or *p*-type Si, leading to the generation of visible photons under IR illumination and the application of an external bias.

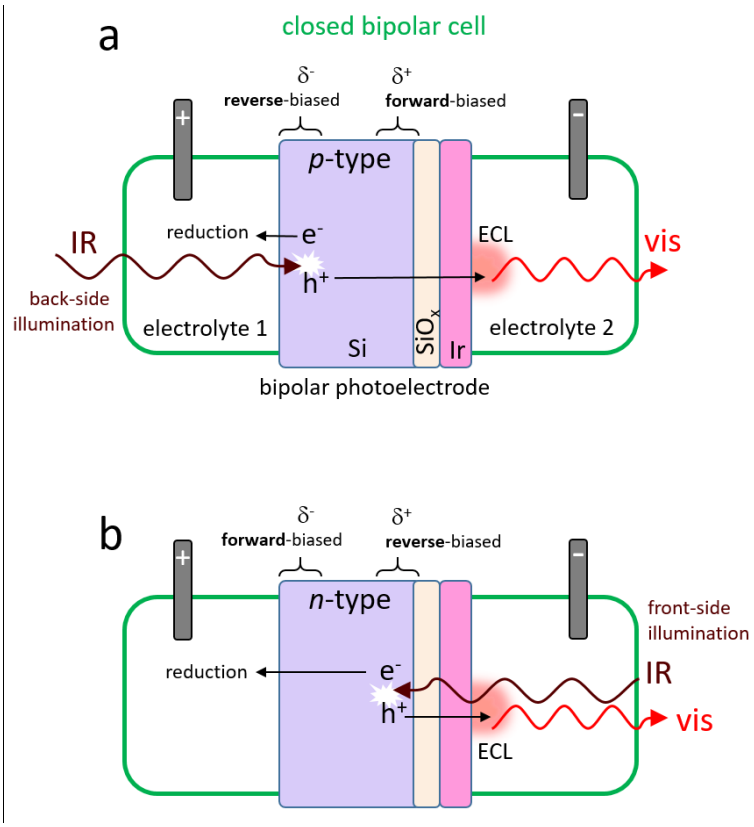

Scheme 1. Up-converting bipolar photoelectrodes. a) *p*-type and b) *n*-type bipolar photoelectrodes operating with back-side and front-side illuminations, respectively.

We used Si as a BPE material, first of all, because of its narrow bandgap (1.1 eV) allowing for anti-Stokes PECL.[14,19–21] Second, because, depending on its doping, Si can be photoinactive (e.g., with heavy n^+-doping) or photoactive, with an electrochemical behavior that can be tuned from photocathodic (with moderate *p*-doping) to photoanodic (with moderate *n*-doping). As shown in **Scheme 1**, two photoactive systems were studied, which differ in the type of doping of the Si BPE: *p*-Si or *n*-Si (n^+-Si was also employed as a non-photoactive reference surface) and in different illumination configurations (back-side or front-side). In this work, we illuminate the photoactive pole of the BPE (the cathodic/anodic pole for the *p*-Si/*n*-Si BPE) so photogenerated minority carriers can readily react with the dissolved species. Back-side illumination refers to the

situation where absorption and PECL emission occur at different sides of the BPE, front-side illumination refers to the situation where absorption and PECL emission occur on the same side. In all cases, the Si BPE (thickness of ~500 μm) separated the two independent electrolyte compartments, each containing a carbon rod feeder electrode connected to an external power supply. The feeder anode compartment was filled with a solution of phosphate buffer saline (PBS) containing 0.2 M $[Fe(CN)_6]^{3-}$ and 0.2 M $[Fe(CN)_6]^{4-}$ (electrolyte 1 in **Scheme 1a**). The feeder cathode compartment was filled with the ECL electrolyte, composed of 5 mM tris(bipyridine)ruthenium(II) ($[Ru(bpy)_3]^{2+}$) and 0.1 M tri-*n*-propylamine (TPrA) in PBS (pH 7.4, electrolyte 2 in **Scheme 1a**), in the first part of this work. Before the experiments, each side of the Si BPE was modified to ensure efficient interfacial charge transfer. The side of the Si surface immersed in the ECL electrolyte (that will be the anodic pole (δ^+) under external polarization) was modified with a protective SiO_x/Ir coating (see SI for more detail) to avoid anodic decomposition during PECL, as recently reported by our group.[21] The side of the Si surface immersed in the $[Fe(CN)_6]^{3-}$/$[Fe(CN)_6]^{4-}$ electrolyte (that will act as the cathodic pole (δ^-)) was freshly hydrogenated with dilute HF to generate Si-H and to remove the native insulating SiO_x layer, which can otherwise impede charge transfer.

Before studying the bipolar cells of **Scheme 1**, each interface was investigated in the dark (dashed lines in **Figure 1**) and under IR illumination (850 nm, solid lines in **Figure 1**) by voltammetry in a conventional 3-electrodes cell connected to a potentiostat. The left part of **Figure 1a-c** (colored in grey) shows the linear sweep voltammograms (LSVs) of 3 types of freshly prepared Si-H cathodes immersed in the $[Fe(CN)_6]^{3-}$/$[Fe(CN)_6]^{4-}$ electrolyte. The right part of the same figure presents LSVs of 3 types of Si/SiO_x/Ir anodes immersed in the $[Ru(bpy)_3]^{2+}$/TPrA ECL electrolyte. We first describe **Figure 1a**, which presents the

electrochemical behavior of n^+-Si-based electrode, a degenerate SC that electrochemically behaves as a conductor. As it can be seen in this panel, n^+-Si-H and n^+-Si/SiO_x/Ir are active in the dark and the IR illumination does not affect their response, in good agreement with the expected behavior for a degenerate SC. Using an arbitrary onset current density of 100 µA cm^{-2}, we can observe that reduction of $[Fe(CN)_6]^{4-}$ occurs at an onset potential of -0.19 V (all potentials in this article are referred vs Ag/AgCl (3 M KCl)) at n^+-Si-H cathodes and the oxidation of the ECL reactants occurs at an onset potential of 0.85 V at n^+-Si/SiO_x/Ir anodes.

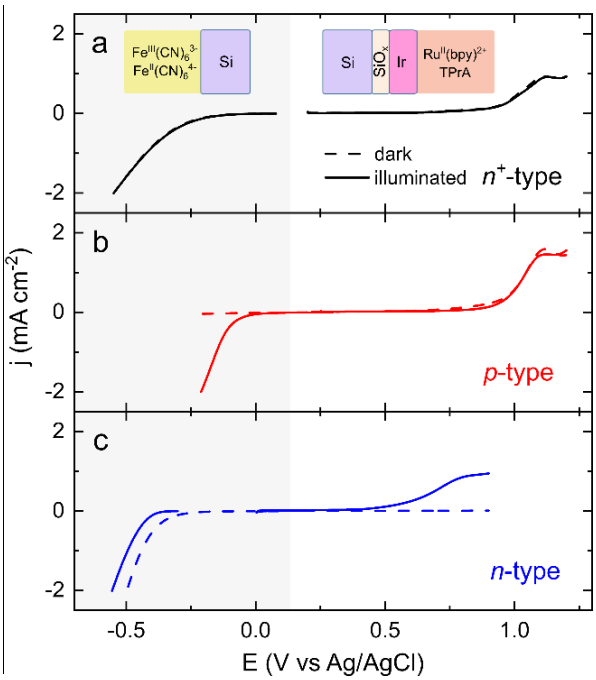

Figure 1. Voltammetric study of the junctions with a three-electrode setup. a) LSVs recorded on n^+-Si-based electrodes. Inset: schemes of the interfaces studied at the electrodes (the Si surface is the working electrode). b) LSVs recorded on *p*-Si-based electrodes. c) LSVs recorded on *n*-Si-based electrodes. LSVs shown in the left (grey square) were obtained at Si-based cathodes in 0.2 M $[Fe(CN)_6]^{3-}$/0.2 M $[Fe(CN)_6]^{4-}$ in PBS. Right LSVs (white square) were obtained at Si/SiO_x/Ir-based anodes in 5 mM $[Ru(bpy)_3]^{2+}$ and 100 mM TPrA in PBS. Full line-LSVs and dashed line-LSVs were recorded under illumination (850 nm) and in the dark, respectively. Scan rate = 50 mV s^{-1}.

Next, the behavior of moderately doped electrodes was studied. As shown in **Figure 1b**, the response of the *p*-Si/SiO_x/Ir anode is not significantly affected by IR illumination and very

similar to that obtained for n^+-Si/SiO_x/Ir (**Figure 1a**). This indicates, that, in this regime, the p-Si/SiO_x/Ir is forward-biased and charge transfer is controlled by majority charge carriers (h^+). It, therefore, behaves as a conventional anode. In contrast, the left part of **Figure 1b** shows that the cathodic behavior for *p*-Si-H is strongly affected by IR illumination. Indeed, this electrode produced a negligible dark current, but a high cathodic photocurrent under illumination. The onset potential for the reduction of $[Fe(CN)_6]^{3-}$ at the illuminated *p*-Si-H, is more positive than that recorded at the non-photoactive n^+-Si-H cathode (**Figure 1a**), due to the generation of a photovoltage at the interface. This behavior is in good agreement with that of a reverse-biased junction exhibiting rectification in the dark and a charge transfer controlled by photogenerated minority carriers (e^-), in other words, a photocathode. *n*-Si-based electrodes were also studied. As shown in **Figure 1c**, in this case, the opposite behavior was observed. Indeed, the *n*-Si-H cathode sustained cathodic current in the dark and under illumination, and the *n*-Si/SiO_x/Ir photoanode exhibited a strong rectification in the dark and a photoactivity under illumination. In the latter case, the ECL onset potential shifted towards a more negative value compared to the non-photoactive n^+-Si/SiO_x/Ir (**Figure 1a**), indicative of conventional photoanode behavior in which the junction is reverse-biased and charge transfer controlled by photogenerated minority carriers (h^+). These experiments showed that *p*-Si and *n*-Si-based surfaces, appropriately treated or coated, behave as photocathodes in the $[Fe(CN)_6]^{3-}$/$[Fe(CN)_6]^{4-}$ electrolyte and photoanodes in the ECL electrolyte, respectively. This is in good agreement with the flatband potential (V_{fb}) values (**Table S1, Figure S1**) obtained by capacitance measurements for the four interfaces based on photoactive Si, which confirm that *p*-Si is in depletion (accumulation) when used as a cathode (anode) and *n*-Si is in depletion (accumulation) when used as an anode (cathode). An

important feature that will be used in the following, is that IR illumination can be used to control the current flow when Si is depleted.

Next, the two interfaces studied in each panel of **Figure 1** were combined to make the BPE assemblies depicted in the inset of **Figure 2a**. In these experiments, the external bias applied between the feeder electrodes was varied and spectra were simultaneously recorded from the δ^+ pole of the BPE using a spectrometer. First, the BPE prepared with non-photoactive n^+-Si was analyzed in the dark. As shown in **Figure 2a**, this BPE generated detectable ECL (red emission with a maximum intensity localized at 630 nm) when the applied bias was higher than 1.7 V. Beyond this, ECL intensity increased with bias, attesting a higher current through the BPE. This value is higher than the threshold required to trigger the redox reactions that can be deduced from the LSV of **Figure 1a** (~1 V, based on the above-mentioned onset potentials). This can be explained by thermodynamic limitations at the feeder cathode, the requirement of reaching a high current density to generate detectable luminescence, and potential losses at the interfaces. The two other configurations, based on moderately doped photoactive Si BPEs, are more interesting as they exhibit a strong dependency on illumination conditions.

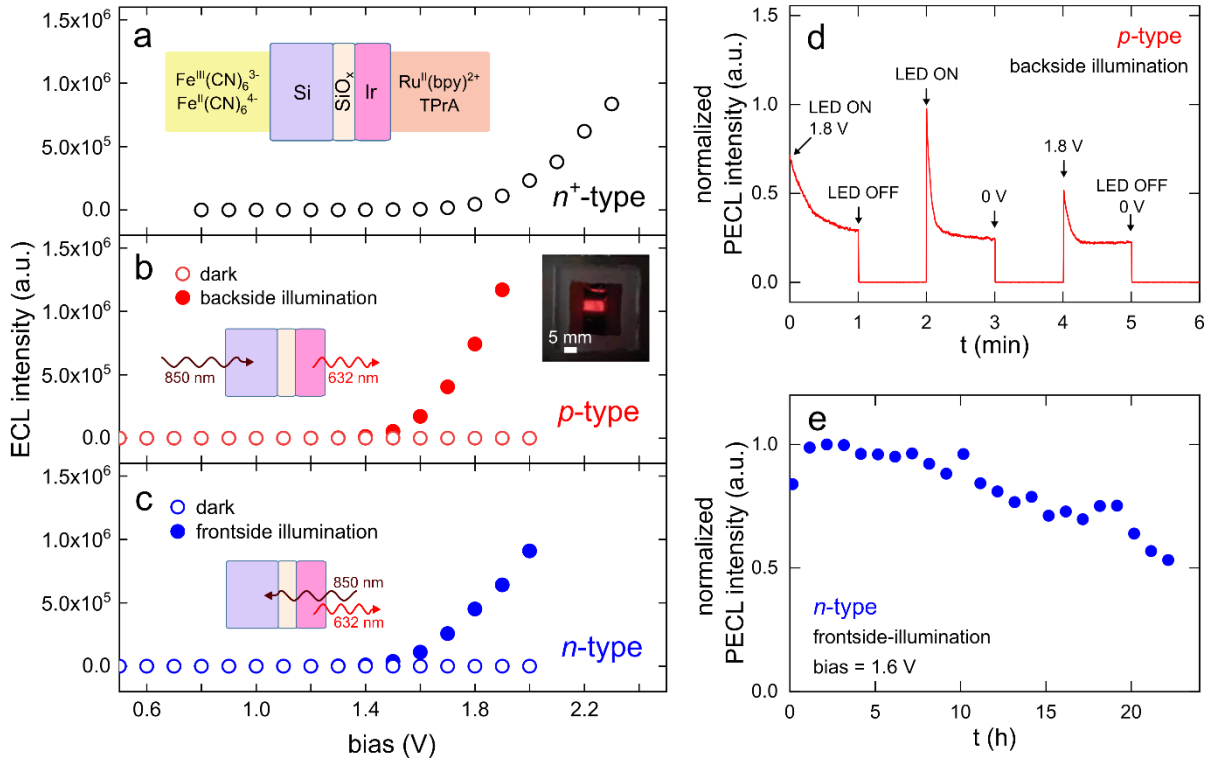

Figure 2. Upconversion PECL at BPEs. a-c) ECL intensity as a function of applied bias for a) an n^+-Si-based BPE in the dark, b) a *p*-Si-based BPE in the dark (empty circles) and under back-side illumination at 850 nm (full circle), and c) an *n*-Si-based BPE in the dark (empty circles) and under front-side illumination at 850 nm (full circle). Left insets in a-c: schemes representing the BPEs and the illumination modes. Right inset in b): photograph showing the PECL emission at the *p*-Si-based BPE. d) PECL intensity recorded at a *p*-Si-based BPE when varying the potential and the light inputs. e) PECL intensity as a function of time for an *n*-Si-based BPE with an applied bias of 1.6 V and a front-side illumination. The electrolytes consist of 0.2 M $[Fe(CN)_6]^{3-}$/0.2 M $[Fe(CN)_6]^{4-}$ in PBS and 5 mM $[Ru(bpy)_3]^{2+}$ and 100 mM TPrA in PBS.

In these experiments, the effect of IR illumination of the photoactive pole of the BPE (δ^- for the *n*-Si BPE, δ^+ for the *p*-Si BPE, as based on the experiments of **Figure 1b,c**) was studied. **Figure 2b** presents the results obtained for a BPE prepared from a *p*-Si substrate. It can be seen here that the BPE is inactive in the dark (empty red circles), due to the rectifying behavior of the reverse-biased *p*-Si-H/electrolyte junction. However, under back-side IR illumination, the BPE

generates PECL at biases higher than 1.4 V (full red circles). This shows that, from that onset bias, electrons photogenerated at the BPE cathodic pole can reduce $[Fe(CN)_6]^{3-}$ and holes can simultaneously induce PECL at the anodic pole. The PECL emission was bright and could be easily visualized with naked eyes, as shown in the inset of **Figure 2b**. **Figure 2c** presents the results obtained for a BPE prepared from an *n*-Si substrate, which has many similarities with the previously described photoactive BPE. Indeed, it is inactive in the dark (empty blue circles), and active under front-side illumination with IR light. Again, PECL is measured at biases higher than 1.4 V (full blue circles), meaning that, above that threshold, photogenerated holes can trigger PECL and electrons can simultaneously reduce $[Fe(CN)_6]^{3-}$. The PECL (produced on photoactive BPEs) starts at a lower applied bias than ECL (produced on the non-photoactive BPE, **Figure 2a**), because of photovoltage generation at the photoactive pole of the BPE. Thus, these BPEs are wireless upconverting systems that can be controlled via two stimuli, i.e., the external bias and IR illumination. This is also clearly seen in **Figure 2d**, which presents the PECL intensity emitted from a *p*-Si BPE as a function of the IR illumination state (on or off) and the external bias (0 or 1.8 V). Here, we can observe that the BPE emits PECL only when both stimuli are applied and that PECL instantaneously responds to bias and illumination. A general concern regarding such systems is their stability because they are based on Si, an unstable electrode material that tends to deactivate, especially when employed for oxidation reactions.[48] As seen in **Figure 2e**, *n*-Si BPEs constantly illuminated and subjected to an external potential of 1.6 V can generate PECL for 22 h, due to the protection provided by the SiO_x/Ir coating.[21] To further elucidate this behavior, simulations were performed for the *n*-Si-based BPE, using the parameters obtained with the three-electrodes setup (**Table S1**, **Figure 1**) and treating the two phases in contact with Si (electrolyte at the δ^- pole and Ir at the δ^+ pole) as Schottky contacts

having a difference in Fermi levels controlled by the external bias. The results, discussed in the supplementary information (**Section 2**), allowed determining the band diagram of the BPE (**Figure S2**) and confirmed that the BPE presents rectification, photoactivity, and decreased onset bias due to photovoltage generation.

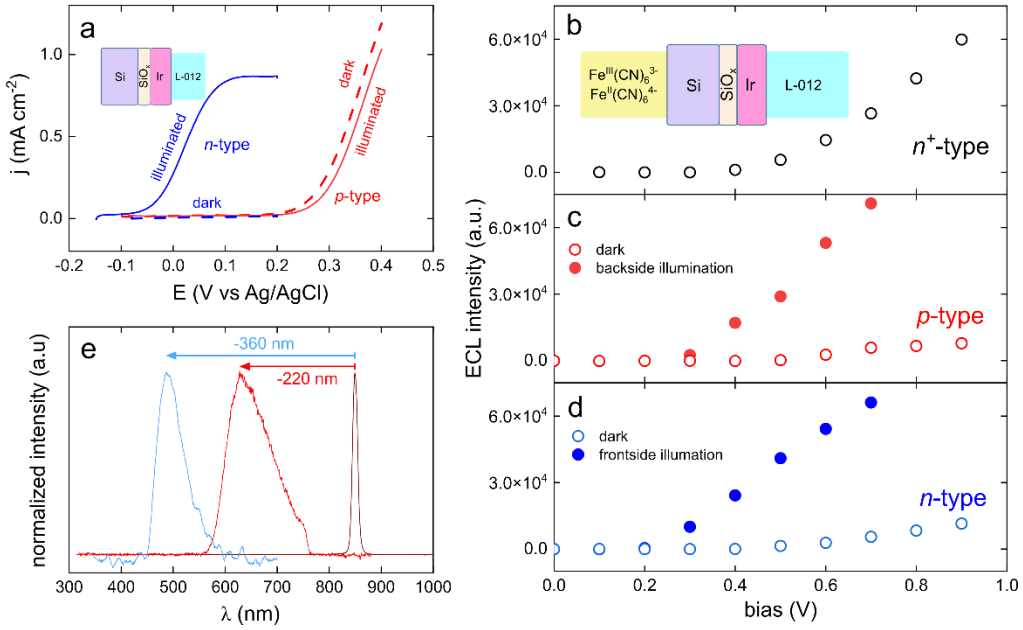

Figure 3. Low-bias upconversion PECL at BPEs. a) LSVs recorded at *n*-Si/SiO_x/Ir (blue) and *p*-Si/SiO_x/Ir (red) the dark (dashed curve) and under illumination (850 nm). The electrolyte was composed of 3 mM L-012 in 0.1 M NaOH, scan rate = 50 mV s^{-1}. Inset represents the interface. b-d) ECL intensity as a function of applied bias for b) an n^+-Si-based BPE in the dark, c) a *p*-Si-BPE in the dark (empty circles) and under back-side illumination at 850 nm (full circle), and d) an *n*-Si-based bipolar photoelectrode in the dark (empty circles) and under back-side illumination at 850 nm (full circle). Inset represents the BPE. e) Normalized spectra of the emission of the LED used in this work (brown spectrum), PECL emission of $[Ru(bpy)_3]^{2+}$(red spectrum), and L-012 (blue spectrum). In b,d) The electrolytes consists of 0.2 M $[Fe(CN)_6]^{3-}$/0.2 M $[Fe(CN)_6]^{4-}$ in PBS and 3 mM L-012 in 0.1 M NaOH.

Finally, our BPE systems were assessed with another ECL electrolyte, that is, a 0.1 M NaOH solution containing 3 mM 8-amino-5-chloro-7-phenyl-pyrido[3,4-d]pyridazine-1,4(2H,3H)dione) (L-012). This luminophore is a luminol analog that emits at 490 nm and that has been previously

used for Stokes-type PECL.[17,18] In addition to its bright ECL emission, a particularity of L-012 is that its oxidation (leading to the ECL emission) occurs at a much lower potential than that of $[Ru(bpy)_3]^{2+}$. Thus, we anticipated that L-012 could be used to trigger wireless PECL with BPEs at a lower applied external bias. As shown in **Figure 3a**, this anodic system was first studied by conventional voltammetry with a 3-electrode setup using *p*- and *n*-Si/SiO_x/Ir anodes. As it was the case previously (**Figure 1b**), *p*-Si/SiO_x/Ir was not photoactive in this potential range and triggered L-012 oxidation with an onset potential of 250 mV. Conversely, *n*-Si/SiO_x/Ir was photoactive and allowed inducing L-012 oxidation at an onset potential as low as -0.03 V under IR illumination. Again, the considerable negative shift of onset potential (-280 mV) is caused by the photovoltage generated at the *n*-Si/SiO_x/Ir junction. Then, BPE systems were designed as previously, except that the $[Ru(bpy)_3]^{2+}$/TPrA ECL electrolyte (electrolyte 2 in **Scheme 1**) was replaced by the L-012 containing electrolyte. **Figure 3b** shows the ECL intensity as a function of the external bias for the non-photoactive n^+-Si-based BPE studied in the dark. Here, ECL can be detected at a bias >0.4 V, a value which is considerably lower compared to that measured (1.7 V) for the non-photoactive BPE operating with $[Ru(bpy)_3]^{2+}$/TPrA (**Figure 2a**). This is caused by the lower thermodynamic threshold required to drive current through the bipolar cell. **Figure 3c** and **3d** present the results obtained with the photoactive *p*-Si and *n*-Si-based BPEs illuminated from the back-side and front-side, respectively. Here, we can see a behavior very similar to that observed previously in **Figure 2b,c** except that the PECL onset is shifted to a lower onset bias. Indeed, the electrodes exhibited a poor activity in the dark, but a strong PECL emission under IR illumination at biases >0.2 V. As shown in **Figure 3e**, in this case, the emission spectrum was shifted to lower wavelengths (maximum emission of 490 nm vs 630 nm for $Ru(bpy)_3]^{2+}$). The anti-Stokes shift can be measured as the difference between the wavelength of maximum

emission (490 nm, blue spectrum in **Figure 3e**) and the excitation wavelength (850 nm, brown spectrum in **Figure 3e**). To the best of our knowledge, this anti-Stokes shift of -360 nm is the largest reported for PECL systems so far.[14]

To conclude, we have reported that closed BPEs based on photoactive *p*- or *n*-Si can be used for the wireless generation of anti-Stokes PECL under IR irradiation with bright emissions in the visible spectrum. The protection of the anodic pole of the BPE with a SiO_x/Ir coating grants stability to the BPE, which can operate for a long time (> 20 h) under illumination. Both illumination modes, front-side and back-side were demonstrated, and, depending on the ECL electrolyte, the onset bias for PECL emission and the anti-Stokes shift can be both tuned. The back-side illumination mode can be particularly interesting for reducing the noise background as, in this case, all the incident light is absorbed by the BPE. In particular, we have shown that using L-012 as a luminophore allows a shift of 360 nm and an onset bias of only 0.2 V. These results present advances for the manufacturing of PECL systems that can operate only with a light stimulus and can be important for the design of chemical sensors or photodetectors.

ASSOCIATED CONTENT

Supporting Information.

The experimental details, the simulation description and results, supplementary figures, and a supplementary table are provided in supporting information.

AUTHOR INFORMATION

Notes

The authors declare no competing financial interests.

ACKNOWLEDGMENT

This work was funded by ANR (LiCORN, ANR-20-CE29-0006).

REFERENCES

(1) Memming, R. *Semiconductor Electrochemistry*; Wiley-VCH, Weinheim, 2015.

(2) Tan, M. X.; Laibinis, P. E.; Nguyen, S. T.; Kesselman, J. M.; Stanton, C. E.; Lewis, N. S. Principles and Applications of Semiconductor Photoelectrochemistry. In *Progress in Inorganic Chemistry*; Karlin, K. D., Ed., Wiley-VCH, Weinheim, 1994; pp 21–144.

(3) Sivula, K.; van de Krol, R. Semiconducting Materials for Photoelectrochemical Energy Conversion. *Nat. Rev. Mater.* **2016**, *1*, 15010.

(4) Fujishima, A.; Honda, K. Electrochemical Photolysis of Water at a Semiconductor Electrode. *Nature* **1972**, *238*, 37–38.

(5) van de Krol, R.; Grätzel, M. *Photoelectrochemical Hydrogen Production*; Springer, New York, 2012.

(6) Walter, M. G.; Warren, E. L.; McKone, J. R.; Boettcher, S. W.; Mi, Q.; Santori, E. A.; Lewis, N. S. Solar Water Splitting Cells. *Chem. Rev.* **2010**, *110*, 6446–6473.

(7) Liu, Z.; Qi, W.; Xu, G. Recent Advances in Electrochemiluminescence. *Chem. Soc. Rev.* **2015**, *44*, 3117–3142.

(8) Sojic, N. *Analytical Electrogenerated Chemiluminescence: From Fundamentals to Bioassays*; The Royal Society of Chemistry, Cambridge, 2020.

(9) Ma, C.; Cao, Y.; Gou, X.; Zhu, J.-J. Recent Progress in Electrochemiluminescence Sensing and Imaging. *Anal. Chem.* **2020**, *92*, 431–454.

(10) Nikolaou, P.; Valenti, G.; Paolucci, F. Nano-Structured Materials for the Electrochemiluminescence Signal Enhancement. *Electrochim. Acta* **2021**, *388*, 138586.

(11) Zanut, A.; Fiorani, A.; Canola, S.; Saito, T.; Ziebart, N.; Rapino, S.; Rebeccani, S.; Barbon, A.; Irie, T.; Josel, H.-P.; Negri, F.; Marcaccio, M.; Windfuhr, M.; Imai, K.; Valenti, G.; Paolucci, F. Insights into the Mechanism of Coreactant Electrochemiluminescence Facilitating Enhanced Bioanalytical Performance. *Nat. Commun.* **2020**, *11*, 2668.

(12) Guo, Y.; Sun, Y.; Zhang, S. Electrochemiluminescence Induced Photoelectrochemistry for Sensing of the DNA Based on DNA-Linked CdS NPs Superstructure with Intercalator Molecules. *Chem. Commun.* **2011**, *47*, 1595–1597.

(13) Zhao, Y.; Yu, J.; Bergamini, J.-F.; Léger, Y.; Sojic, N.; Loget, G. Photoelectrochemistry at Semiconductor/Liquid Interfaces Triggered by Electrochemiluminescence. *Cell Reports Phys. Sci.* **2021**, 100670.

(14) Zhao, Y.; Bouffier, L.; Xu, G.; Loget, G.; Sojic, N. Electrochemiluminescence with Semiconductor (Nano)Materials. *Chem. Sci.* **2022**, *13*, 2528–2550.

(15) Laser, D.; Bard, A. J. Semiconductor Electrodes. Photo-Induced Electrogenerated

Chemiluminescence and up-Conversion at Semiconductor Electrodes. *Chem. Phys. Lett.* **1975**, *34*, 605–610.

(16) Luttmer, J. D.; Bard, A. J. Electrogenerated Chemiluminescence: 34. Photo- Induced Electrogenerated Chemiluminescence and Up- Conversion at Semiconductor Electrodes. *J. Electrochem. Soc.* **1979**, *126*, 414–419.

(17) Yu, J.; Saada, H.; Abdallah, R.; Loget, G.; Sojic, N. Luminescence Amplification at $BiVO_4$ Photoanodes by Photoinduced Electrochemiluminescence. *Angew. Chemie Int. Ed.* **2020**, *59*, 15157–15160.

(18) Yu, J.; Saada, H.; Sojic, N.; Loget, G. Photoinduced Electrochemiluminescence at Nanostructured Hematite Electrodes. *Electrochim. Acta* **2021**, *381*, 138238.

(19) Vogel, Y. B.; Darwish, N.; Ciampi, S. Spatiotemporal Control of Electrochemiluminescence Guided by a Visible Light Stimulus. *Cell Reports Phys. Sci.* **2020**, *1*, 100107.

(20) Zhao, Y.; Yu, J.; Xu, G.; Sojic, N.; Loget, G. Photoinduced Electrochemiluminescence at Silicon Electrodes in Water. *J. Am. Chem. Soc.* **2019**, *141*, 13013–13016.

(21) Zhao, Y.; Descamps, J.; Ababou-Girard, S.; Bergamin, J.-F.; Santinacci, L.; Léger, Y.; Sojic, N.; Loget, G. Metal-Insulator-Semiconductor Anodes for Ultrastable and Site-Selective Upconversion Photoinduced Electrochemiluminescence. *Angew. Chem. Int. Ed.* **2022**, 61, e202201865.

(22) Fosdick, S. E.; Knust, K. N.; Scida, K.; Crooks, R. M. Bipolar Electrochemistry. *Angew.*

Chemie Int. Ed. **2013**, *52*, 10438–10456.

(23) Bouffier, L.; Zigah, D.; Sojic, N.; Kuhn, A. Bipolar Electrochemistry. In *Encyclopedia of Electrochemistry*.Wiley-VCH, Weinheim, 2021, pp 1–53.

(24) Crooks, R. M. Principles of Bipolar Electrochemistry. *ChemElectroChem* **2016**, *3*, 357–359.

(25) Loget, G.; Zigah, D.; Bouffier, L.; Sojic, N.; Kuhn, A. Bipolar Electrochemistry: From Materials Science to Motion and Beyond. *Acc. Chem. Res.* **2013**, *46*, 2513–2523.

(26) Bradley, J.-C.; Chen, H.-M.; J., C.; Eckert, J.; Ernazarova, K.; Kurzeja, T.; Lin, M.; McGee, M.; Nadler, W.; Stephens, S. G. Creating Electrical Contacts between Metal Particles Using Directed Electrochemical Growth. *Science.* **1997**, *389*, 268–271.

(27) Loget, G.; So, S.; Hahn, R.; Schmuki, P. Bipolar Anodization Enables the Fabrication of Controlled Arrays of TiO_2 Nanotube Gradients. *J. Mater. Chem. A* **2014**, *2*, 17740–17745.

(28) Gupta, B.; Zhang, L.; Melvin, A. A.; Goudeau, B.; Bouffier, L.; Kuhn, A. Designing Tubular Conducting Polymer Actuators for Wireless Electropumping. *Chem. Sci.* **2021**, *12*, 2071–2077.

(29) Bouffier, L.; Zigah, D.; Sojic, N.; Kuhn, A. Bipolar (Bio)Electroanalysis. *Annu. Rev. Anal. Chem.* **2021**, *14*, 65–86.

(30) Rahn, K. L.; Anand, R. K. Recent Advancements in Bipolar Electrochemical Methods of Analysis. *Anal. Chem.* **2021**, *93*, 103–123.

(31) Gamero-Quijano, A.; Molina-Osorio, A. F.; Peljo, P.; Scanlon, M. D. Closed Bipolar

Electrochemistry in a Four-Electrode Configuration. *Phys. Chem. Chem. Phys.* **2019**, *21*, 9627–9640.

(32) Loget, G.; Li, G.; Fabre, B. Logic Gates Operated by Bipolar Photoelectrochemical Water Splitting. *Chem. Commun.* **2015**, *51*, 11115–11118.

(33) Loget, G.; Fabre, B. Light-Driven Bipolar Electrochemical Logic Gates with Electrical or Optical Outputs. *ChemElectroChem* **2016**, *3*, 366–371.

(34) Melvin, A. A.; Gupta, B.; Tieriekhov, K.; Nogala, W.; Garrigue, P.; Reculusa, S.; Kuhn, A. Wireless Dual Stimuli Actuation of Dye Sensitized Conducting Polymer Hybrids. *Adv. Funct. Mater.* **2021**, *31*, 2101171.

(35) Ongaro, M.; Roche, J.; Kuhn, A.; Ugo, P. Asymmetric Modification of TiO_2 Nanofibers with Gold by Electric-Field-Assisted Photochemistry. *ChemElectroChem* **2014**, *1*, 2048–2051.

(36) Tiewcharoen, S.; Warakulwit, C.; Lapeyre, V.; Garrigue, P.; Fourier, L.; Elissalde, C.; Buffière, S.; Legros, P.; Gayot, M.; Limtrakul, J.; Kuhn, A. Anisotropic Metal Deposition on TiO_2 Particles by Electric-Field-Induced Charge Separation. *Angew. Chemie Int. Ed.* **2017**, *56*, 11431–11435.

(37) Zhan, W.; Alvarez, J.; Crooks, R. M. Electrochemical Sensing in Microfluidic Systems Using Electrogenerated Chemiluminescence as a Photonic Reporter of Redox Reactions. *J. Am. Chem. Soc.* **2002**, *124*, 13265–13270.

(38) Wu, M.-S.; Yuan, D.-J.; Xu, J.-J.; Chen, H.-Y. Electrochemiluminescence on Bipolar

Electrodes for Visual Bioanalysis. *Chem. Sci.* **2013**, *4*, 1182–1188.

(39) Li, H.; Bouffier, L.; Arbault, S.; Kuhn, A.; Hogan, C. F.; Sojic, N. Spatially-Resolved Multicolor Bipolar Electrochemiluminescence. *Electrochem. commun.* **2017**, *77*, 10–13.

(40) de Poulpiquet, A.; Diez-Buitrago, B.; Dumont Milutinovic, M.; Sentic, M.; Arbault, S.; Bouffier, L.; Kuhn, A.; Sojic, N. Dual Enzymatic Detection by Bulk Electrogenerated Chemiluminescence. *Anal. Chem.* **2016**, *88*, 6585–6592.

(41) Wang, Y.; Jin, R.; Sojic, N.; Jiang, D.; Chen, H.-Y. Intracellular Wireless Analysis of Single Cells by Bipolar Electrochemiluminescence Confined in a Nanopipette. *Angew. Chemie Int. Ed.* **2020**, *59*, 10416–10420.

(42) Sentic, M.; Loget, G.; Manojlovic, D.; Kuhn, A.; Sojic, N. Light-Emitting Electrochemical "Swimmers." *Angew. Chem. Int. Ed.* **2012**, *51*, 11284–11288.

(43) Eßmann, V.; Voci, S.; Loget, G.; Sojic, N.; Schuhmann, W.; Kuhn, A. Wireless Light-Emitting Electrochemical Rotors. *J. Phys. Chem. Lett.* **2017**, *8*, 4930–4934.

(44) Villani, E.; Inagi, S. Mapping the Distribution of Potential Gradient in Bipolar Electrochemical Systems through Luminol Electrochemiluminescence Imaging. *Anal. Chem.* **2021**, *93*, 8152–8160.

(45) Anderson, T. J.; Defnet, P. A.; Zhang, B. Electrochemiluminescence (ECL)-Based Electrochemical Imaging Using a Massive Array of Bipolar Ultramicroelectrodes. *Anal. Chem.* **2020**, *92*, 6748–6755.

(46) Ismail, A.; Voci, S.; Pham, P.; Leroy, L.; Maziz, A.; Descamps, L.; Kuhn, A.; Mailley, P.;

Livache, T.; Buhot, A.; Leichlé, T.; Bouchet-Spinelli, A.; Sojic, N. Enhanced Bipolar Electrochemistry at Solid-State Micropores: Demonstration by Wireless Electrochemiluminescence Imaging. *Anal. Chem.* **2019**, *91*, 8900–8907.

(47) Qin, X.; Jin, H.-J.; Li, X.; Li, J.; Pan, J.-B.; Wang, K.; Liu, S.; Xu, J.-J.; Xia, X.-H. Label-Free Electrochemiluminescence Imaging of Single-Cell Adhesions by Using Bipolar Nanoelectrode Array. *Chem. Eur. J.* **2022**, *28*, e202103964.

(48) Bae, D.; Seger, B.; Vesborg, P. C. K.; Hansen, O.; Chorkendorff, I. Strategies for Stable Water Splitting via Protected Photoelectrodes. *Chem. Soc. Rev.* **2017**, *46*, 1933–1954.